

## Formation and Catalysis of Mesoporous Nb–Mo Oxide Generated by the Self-assembly of Nanoparticles

Kazu Okumura,<sup>\*1</sup> Soichiro Ishida,<sup>1</sup> Yoshitaka Kinoshita,<sup>1</sup> Takashi Sanada,<sup>1,2</sup> Keiko Iida,<sup>2</sup> and Naonobu Katada<sup>1</sup>  
<sup>1</sup>Department of Chemistry and Biotechnology, Graduate School of Engineering, Tottori University, Tottori 680-8552  
<sup>2</sup>Research Department, NISSAN ARC, LTD., Yokosuka, Kanagawa 237-0061

(Received June 22, 2012; CL-120673; E-mail: okmr@chem.tottori-u.ac.jp)

Mesoporous solid acid catalyst composed of Nb–Mo oxide was prepared via a hydrothermal synthesis employing ammonium niobium oxalate and hexaammonium heptamolybdate tetrahydrate as the precursors. The assembly of fine particles with diameters of 20–34 nm was observed by field emission–scanning electron microscopy. The Nb–Mo oxide has mesopores with diameters of 1.6–2.0 nm. It was possible to tune size of the primary particles and diameter of the mesopores by changing Mo/Nb ratio. The Nb–Mo oxide exhibited high activity in Friedel–Crafts alkylation.

Mesoporous materials have received considerable attention after the discovery of MCM-41 and FSM-16.<sup>1,2</sup> The presence of mesopores is beneficial for the promotion of reactions, because regular mesopores promote the diffusion of molecules. Synthesis of mesoporous materials has been extended to other kinds of elements including Al<sub>2</sub>O<sub>3</sub>, Nb<sub>2</sub>O<sub>5</sub>, and Ta<sub>2</sub>O<sub>5</sub>.<sup>3–5</sup> Nb–Mo- or Nb-based mesoporous oxides have also been synthesized using triblock copolymers as templates.<sup>6</sup> These catalysts have been successfully applied to the Friedel–Crafts alkylation of anisole. In general, templates including ammonium salts and surfactants have been utilized for the synthesis of mesoporous materials. It is necessary to remove the template molecules through calcination or extraction in order to obtain mesoporosity. We have recently reported that the posttreatment of hydrothermally synthesized Nb<sub>2</sub>O<sub>5</sub>–WO<sub>x</sub> with an aqueous solution of oxalic acid resulted in the formation of a layered structure in which fibrous oxide was assembled.<sup>7</sup> This finding suggests a new methodology for the synthesis of porous materials through self-assembly of primary particles, as reported in silica materials.<sup>8</sup> Here, we report that a mesoporous Nb–Mo oxide could be synthesized through the self-assembly of nanoparticles without the addition of templates.

Nb–Mo oxide was synthesized using a hydrothermal method: In a typical synthesis, a solution of hexaammonium heptamolybdate tetrahydrate, (NH<sub>4</sub>)<sub>6</sub>Mo<sub>7</sub>O<sub>24</sub>·4H<sub>2</sub>O (Wako Chemical Co., 5.49 g), dissolved in water (60 mL) was mixed in a flask with ammonium niobium oxalate, NH<sub>4</sub>[NbO(C<sub>2</sub>O<sub>4</sub>)<sub>2</sub>(H<sub>2</sub>O)]·xH<sub>2</sub>O (CBMM Co., 0.53–4.12 g), dissolved in water (10 mL), and then the gas phase was purged with N<sub>2</sub>. The total concentration of metals (Nb and Mo) was fixed at 0.124 mol L<sup>-1</sup>, while the Mo/Nb ratio was varied from 1.5 to 20. The mixed solution was placed in a Teflon-sealed autoclave in a glove box under N<sub>2</sub>. Catalyst preparation was carried out at 443 K for 48 h while the autoclave was continuously rotated at a speed of 15 rpm. The solid (denoted as NbMo hereinafter) was separated from the solution by suction filtration using a membrane filter or centrifugation. The separated solid was thoroughly washed with water, after which it was calcined in a N<sub>2</sub> flow (50 mL min<sup>-1</sup>) at 573 K for 2 h prior to characterization and used for the catalytic reaction. The prepared sample will be denoted as NbMo-*x*, where *x* denotes the Mo/(Mo + Nb) ratio of the obtained solid.

After the hydrothermal synthesis, a dark blue solid was observed as turbidity in the water, because the deposition of the as-prepared NbMo was slow as a result of the formation of fine particles.<sup>9</sup> The yield of the NbMo was in the range of 16%–94%; the value increased with decreasing in the Mo/Nb ratio. The obtained NbMo was separated by filtration or centrifugation. After it was dried, the NbMo formed black, shiny grains.<sup>9</sup> The dried NbMo precipitated on the bottom of the flask immediately in water, even after stirring due to the formation of aggregated solids. The features of the NbMo did not change after it was stirred in boiling water. The change in the nature of NbMo caused by the drying procedure suggests the presence of a cohesive interaction between primary particles. The composition of the NbMo was measured by means of inductively coupled plasma after dissolution of the NbMo in an aqueous solution of oxalic acid.

The Mo/(Mo + Nb) ratios of the NbMo samples prepared with mother solutions with Mo/(Mo + Nb) = 0.6, 0.75, 0.83, 0.91, and 0.95 were 0.56, 0.66, 0.69, 0.73, and 0.75, respectively. This means that Nb was preferentially incorporated in NbMo during hydrothermal synthesis. Figures 1a and 1b show field emission–scanning electron microscopy (FE-SEM) images of NbMo-0.73. It can be seen in the figures that the fine particulates with ca. 30-nm diameter were closely packed to form a flat surface. Figure 1c shows an FE-SEM image of NbMo-0.56. The image was taken with the same magnification as Figure 1b. The particles assembled to form a grain in a similar manner to that observed for NbMo-0.73, but it is obvious that the NbMo-0.56 particles were smaller than the NbMo-0.73 particles. The average sizes of the particles are summarized in Table 1. The size became smaller with increasing Nb content in the NbMo. In contrast to the NbMo, single components (Nb or Mo oxide) did not form such fine particles after hydrothermal synthesis. Nitrogen adsorption isotherms and the pore size distribution calculated based on the desorption branches according to the Barrett–Joyner–Halenda (BJH) method are displayed in Figure 2. The isotherms were categorized as type IV, meaning that mesopores were present. Hysteresis was observed in the isotherms between the adsorption and desorption branches, suggesting the presence of mesopores with ink-bottle-like shapes. It can be seen in the isotherms that the second increase in the nitrogen adsorption shifted with increasing Nb content. The distribution of the mesopore sizes in NbMo was narrow, with a mean size of 1.6–2.1 nm (Figure 2b). The diameters of the mesopores became smaller with increasing Nb content in the NbMo. In other words, the mean size of the mesopores could be regulated by changing the Mo/Nb ratio of NbMo. Because the mean particle size tended to become smaller with increasing Nb content, the origin of the mesopores may be the space between the NbMo particles. The specific surface area calculated using the BET method was 130–226 m<sup>2</sup> g<sup>-1</sup> (Table 1). The highest value was obtained in NbMo-0.69 and -0.73. This value seems to be high, considering that the

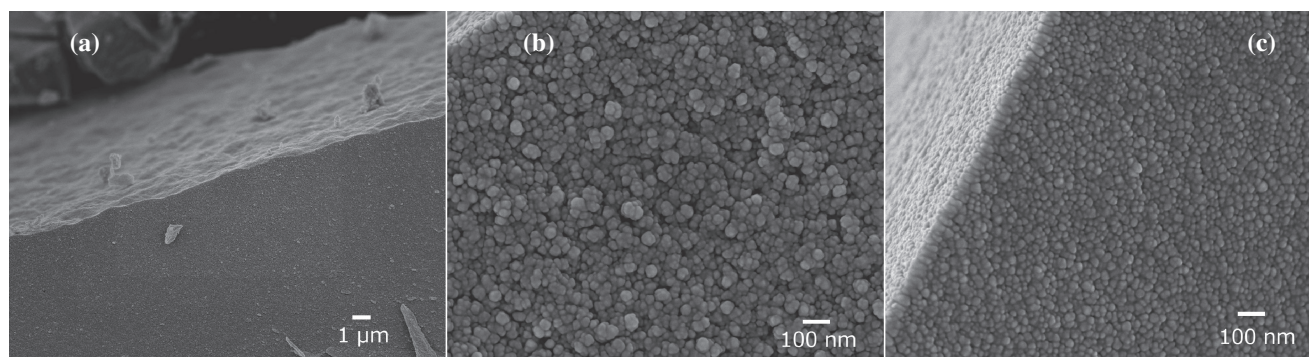


**Figure 1.** FE-SEM images of (a, b) NbMo-0.73 and (c) NbMo-0.56.

**Table 1.** Textural properties and acid amounts of NbMo

| Mo/<br>(Mo + Nb) | Mean<br>particle<br>size/nm <sup>a</sup> | Specific<br>surface<br>area/m <sup>2</sup> g <sup>-1b</sup> | Pore<br>volume<br>/cm <sup>3</sup> g <sup>-1b</sup> | Acid<br>amount<br>/mol kg <sup>-1c</sup> |
|------------------|--|---|---|--|
| 0.56             | 20                                       | 130   | 0.09  | 0.91                                     |
| 0.66             | 22                                       | 163   | 0.11  | 0.96                                     |
| 0.69             | 22                                       | 226   | 0.20  | 0.94                                     |
| 0.73             | 27                                       | 224   | 0.25  | 1.20                                     |
| 0.75             | 34                                       | 165   | 0.19  | 1.18                                     |

<sup>a</sup>Determined with FE-SEM images. <sup>b</sup>Calculated based on the N<sub>2</sub> adsorption isotherms. <sup>c</sup>Determined with NH<sub>3</sub> TPD.

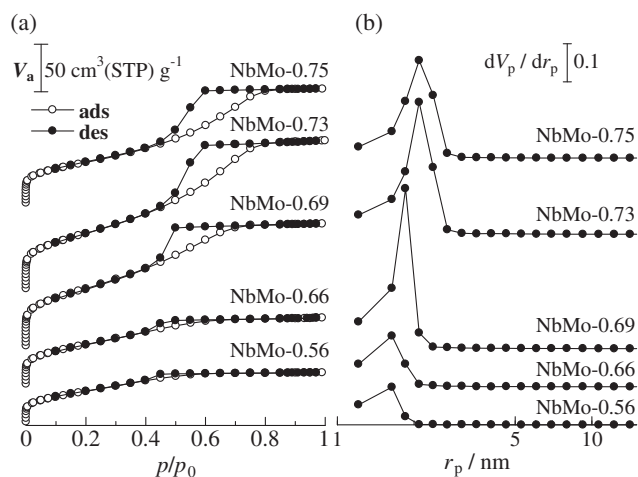


**Figure 2.** (a) N<sub>2</sub> adsorption isotherms and (b) pore size distribution calculated based on the desorption branches according to the BJH method.

NbMo was synthesized without the addition of template molecules.

The X-ray diffraction (XRD) patterns of uncalcined NbMo-0.73 and NbMo-0.73 samples calcined in a stream of N<sub>2</sub> at different temperatures from 473 to 873 K are displayed in Figure 3. Two peaks appeared at 22.2 and 45.2° for the NbMo-0.73 calcined at 473–773 K and for the uncalcined sample. The diffraction changed after calcination in a stream of N<sub>2</sub> at 873 K. The peak positions of the newly appearing peaks are consistent with those of Mo<sub>3</sub>Nb<sub>2</sub>O<sub>14</sub>.<sup>10</sup> Therefore, the two peaks appearing at 22.2 and 45.2° were tentatively assigned to the (001) and (002) of Mo<sub>3</sub>Nb<sub>2</sub>O<sub>14</sub>.

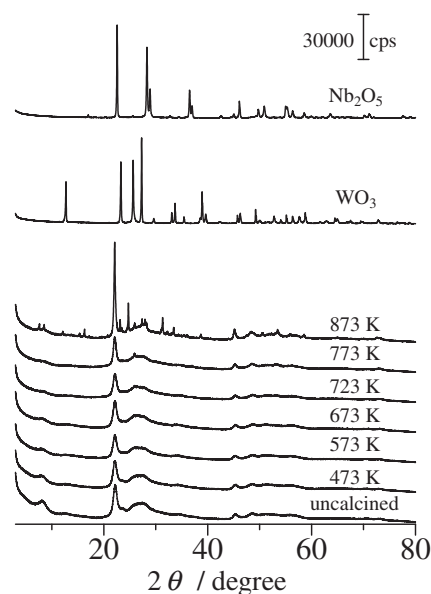


**Figure 3.** XRD patterns of NbMo-0.73 calcined at different temperatures and reference samples.

Figure 4 displays the TEM image of NbMo-0.73. The particles composed a small domain with diameter of ca. 5 nm as displayed by the circle in Figure 4. A fringe pattern can be seen in the domain. The lattice spacing was measured to be 0.39 nm. The spacing agrees with the lattice spacing in *c* axis of Mo<sub>3</sub>Nb<sub>2</sub>O<sub>14</sub> reported in the literature,<sup>10</sup> indicating the 5-nm-sized crystals assembled in a particle.

The acidic properties of NbMo were characterized by the temperature-programmed desorption of ammonia (NH<sub>3</sub>-TPD). Broad ammonia desorption signals were observed in the temperature range between 400 and 700 K (Figure 5a). A small peak overlapped these broad signals at 600–700 K. The shoulder was pronounced for the NbMo-0.56, -0.66, and -0.75. The change in the shape of TPD suggested that the acid property was dependent on the composition of the Nb–Mo oxide. Figure 5b shows the FT-IR of NbMo-0.73 measured during NH<sub>3</sub>-TPD. The bending mode of NH<sub>3</sub> adsorbed on Lewis acid sites (1250 and 1610 cm<sup>-1</sup>) diminished at 573 K along with increase in temperature. On the other hand, NH<sub>4</sub><sup>+</sup> on Brønsted acid sites (1420 cm<sup>-1</sup>) remained at 573 K. This indicated that the primary peak in NH<sub>3</sub>-TPD was due to a mixture of Brønsted and Lewis sites, while the shoulder appearing at higher temperature was due to Brønsted sites. The

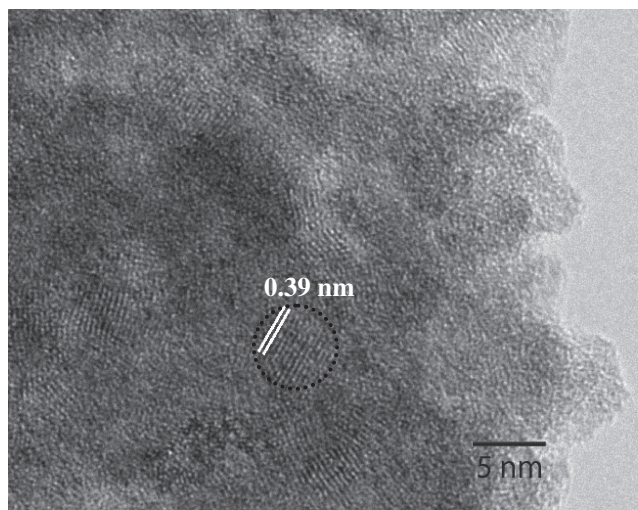


Figure 4. TEM image of NbMo-0.73.

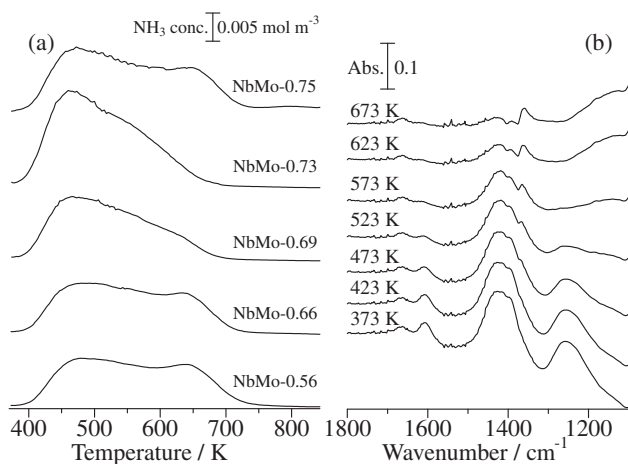


Figure 5. (a)  $\text{NH}_3$  TPD of NbMo-0.56–0.75, (b) FT-IR spectra of NbMo-0.73 measured during  $\text{NH}_3$  TPD.

total amounts of desorbed ammonia were in the range 0.91–1.20 mol kg<sup>-1</sup> (Table 1). The largest amount of acid was obtained for NbMo-0.73 (1.20 mol kg<sup>-1</sup>). For this sample, the density of the adsorbed ammonia was calculated to be 3.3 nm<sup>-2</sup> based on the amount of desorbed  $\text{NH}_3$  and the specific surface area (224 m<sup>2</sup> g<sup>-1</sup>). The origin of acidity of Nb–Mo oxide is not clearly revealed at this stage. However, one hypothesis is the stabilization of Mo(V) in place of Mo(VI) brought about the formation of Brønsted acid sites ( $\text{H}^+$ ) which compensated the charge balance. In agreement with this assumption, formation of the Mo(V) and a hole in  $\text{Mo}_3\text{Nb}_2\text{O}_{14}$  has been reported in the literature.<sup>10</sup> Moreover, acid amount of NbMo-0.73 decreased after calcination in  $\text{O}_2$  at 573 K (0.67 mol kg<sup>-1</sup>). This suggested that the Mo(V) was responsible for the evolution of Brønsted acidity of Nb–Mo oxide.

Catalytic reactions utilizing the acid sites were performed over NbMo after it was calcined in a flow of  $\text{N}_2$  at 573 K in order to eliminate the  $\text{NH}_4^+$  remaining on the NbMo surface, as confirmed by infrared spectra.<sup>9</sup> The remaining  $\text{NH}_4^+$  was supposed to originate from the Nb precursor ( $\text{NH}_4[\text{NbO}(\text{C}_2\text{O}_4)_2 \cdot$

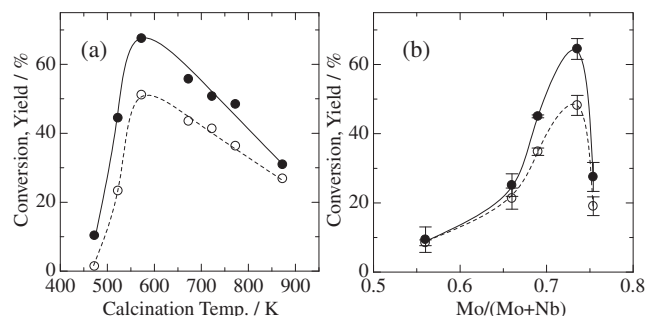


Figure 6. Friedel–Crafts alkylation of anisole with benzyl alcohol (●: benzyl alcohol conversion; ○: benzyanisole yield). Dependence on the (a) calcination temperature over NbMo-0.73, (b) composition of NbMo. Catalyst weight, 30 mg; anisole, 10 g; benzyl alcohol, 0.675 g; temp, 373 K; time, 3 h.

( $\text{H}_2\text{O}$ ) $\cdot x\text{H}_2\text{O}$ ). Figure 6a shows catalytic activity of NbMo-0.73 plotted as a function of calcination temperature. The highest activity was obtained after calcination at 573 K, the temperature agreed with that of the removal of  $\text{NH}_4^+$ . The activity declined on further increase in the calcination temperature, probably due to the lowering of surface area. Dependence of the catalytic activity on the NbMo composition is given in Figure 6b. The maximum activity was attained for NbMo-0.73. The acid sites corresponding to the desorption peak at ca. 460 K in  $\text{NH}_3$ -TPD were presumably responsible for the evolution of the catalytic activity, taking into account that the samples were pretreated at 573 K. The amount of desorption from ca. 460 K was the highest in NbMo-0.73 among prepared samples. The catalytic activity of NbMo-0.73 was as much as twice that of  $\beta$ -zeolite ( $\text{H}\beta$ -20,  $\text{Si}/\text{Al}_2 = 25$ , supplied from PQ company).<sup>11</sup>

In conclusion, we found that the hydrothermally synthesized Nb–Mo oxides aggregated to form ordered mesoporous solids. The size of the primary particles and the mesopore size could be regulated by changing the Mo/Nb ratio. This suggests that Nb–Mo oxide is a promising acidic catalyst.

#### References and Notes

- J. S. Beck, J. C. Vartuli, W. J. Roth, M. E. Leonowicz, C. T. Kresge, K. D. Schmitt, C. T.-W. Chu, D. H. Olson, E. W. Sheppard, S. B. McCullen, J. B. Higgins, J. L. Schlenker, *J. Am. Chem. Soc.* **1992**, *114*, 10834.
- S. Inagaki, A. Koiwai, N. Suzuki, Y. Fukushima, K. Kuroda, *Bull. Chem. Soc. Jpn.* **1996**, *69*, 1449.
- Z. Zhang, R. W. Hicks, T. R. Pauly, T. J. Pinnavaia, *J. Am. Chem. Soc.* **2002**, *124*, 1592.
- K. Brezesinski, J. Wang, J. Haetge, C. Reitz, S. O. Steinmueller, S. H. Tolbert, B. M. Smarsly, B. Dunn, T. Brezesinski, *J. Am. Chem. Soc.* **2010**, *132*, 6982.
- Y. Takahara, J. N. Kondo, T. Takata, D. Lu, K. Domen, *Chem. Mater.* **2001**, *13*, 1194.
- C. Tagusagawa, A. Takagaki, A. Iguchi, K. Takanabe, J. N. Kondo, K. Ebitani, T. Tatsumi, K. Domen, *Catal. Today* **2011**, *164*, 358.
- K. Okumura, S. Ishida, T. Tomiyama, M. Niwa, *Chem. Lett.* **2011**, *40*, 527.
- T. Yokoi, Y. Sakamoto, O. Terasaki, Y. Kubota, T. Okubo, T. Tatsumi, *J. Am. Chem. Soc.* **2006**, *128*, 13664.
- Supporting Information is available electronically on the CSJ-Journal Web site, <http://www.csj.jp/journals/chem-lett/index.html>.
- P. Afanasiev, *J. Phys. Chem. B* **2005**, *109*, 18293.
- U. Freese, F. Heinrich, F. Roessner, *Catal. Today* **1999**, *49*, 237.